Journal of Alloys and Compounds 512 (2012) 223–229

Contents lists available at SciVerse ScienceDirect

Journal of Alloys and Compounds

journal homepage: www.elsevier.com/locate/jallcom

Preparation, crystal structure and photoluminescence of lithium magnesium manganese borate solid solutions, $LiMg_{1-x}Mn_xBO_3$

Hisanori Yamane[a,*], Tetsuya Kawano[a], Kentaro Fukuda[b], Takayuki Suehiro[a], Tsugio Sato[a]

[a] Institute of Multidisciplinary Research for Advanced Materials, Tohoku University, 2-1-1 Katahira, Aoba-ku, Sendai 980-8577, Japan
[b] TOKUYAMA Corporation, 1-1, Harumi-cho, Shunan-shi, Yamaguchi 745-0024, Japan

ARTICLE INFO

Article history:
Received 13 July 2011
Received in revised form
20 September 2011
Accepted 22 September 2011
Available online 29 September 2011

Keywords:
Optical materials
Oxide materials
Nuclear reactor materials
Solid state reaction
Crystal growth
Crystal structure
X-ray diffraction
Luminescence

ABSTRACT

$LiMg_{1-x}Mn_xBO_3$ solid solutions were prepared by solid state reaction in Ar at 800 °C. The X-ray diffraction reflections of the solid solutions with the manganese content x from 0 to 0.5 were indexed with monoclinic cells (space group $C2/c$ (No. 15)). The solid solution of $x = 0.75$ has the hexagonal structure of $LiMnBO_3$ (space group $P\bar{6}$ (No. 174)). Colorless transparent platelet single crystals of $LiMg_{0.5}Mn_{0.5}BO_3$ were prepared by heating a polycrystalline sample of $x = 0.50$ with a Li_2BO_2 flux and by slow cooling from 900 °C. The crystal structure was analyzed by single crystal X-ray diffraction (monoclinic, $C2/c$, $a = 5.1820(2)$ Å, $b = 8.9241(4)$ Å, $c = 10.1529(6)$ Å, $\beta = 91.5824(18)°$, $R1 = 0.0271$, $wR2 = 0.0645$, and $S = 1.219$ for all data). Mn^{2+} and Mg^{2+} atoms statistically occupy a 5-fold coordinate site of oxygen trigonal bipyramid. Monoclinic $LiMg_{1-x}Mn_xBO_3$ solid solutions emit red light with a peak wavelength $\lambda_{em} = 682$–696 nm due to d–d transition under visible light of 428 nm at room temperature. The radiation lifetimes decreased from 24 ms to 0.3 ms with increasing x from 0.02 to 0.30. Stronger red emission of 698 nm was observed for the sample of $x = 0.10$ by excitation of ultraviolet light $\lambda_{ex} = 200$ nm.

1. Introduction

Various kinds of luminescent materials have been developed by doping Mn^{2+} into host crystals of oxides, fluorides, sulfides, and so on [1,2]. The luminescent color of Mn^{2+} activators is changed from green to red by the coordination number and environment in the host crystals. The process of the light emission is spin forbidden d–d transition of $^4T_1(G)$–$^6A_1(S)$, and the decay time of Mn^{2+} luminescence is usually in the millisecond range [2].

$Cd_2B_2O_5$:Mn^{2+} is a borate phosphor which had been used for fluorescence lamps, emitting red light with a peak wavelength (λ_{em}) of 620–626 nm with over 90% quantum efficiency under ultraviolet (UV) light irradiation of 254 nm [3,4]. Kawano et al. synthesized magnesium manganese pyroborate $(Mg_{1-x}Mn_x)_2B_2O_5$ solid solutions and reported the crystal structure and luminescence properties [5]. Deep red color emission of 670 nm from the pyroborate was observed by irradiating visible light of 414 nm. Recently, $(Mg_{0.95}Mn_{0.05})_2B_2O_5$ was prepared with ^{10}B which has a high neutron-capture cross-section σ (3840 barn for thermal neutron). The deep red light is also emitted by α-ray irradiation. A neutron detector was set by combination of a 0.2 mm thick ceramic plate of $(Mg_{0.95}Mn_{0.05})_2B_2O_5$ and a Si photodiode. It was demonstrated that the ceramics can be used as neutron scintillator with low noise by γ ray due to the light constituent elements of Mg, B, and O [6]. Lithium-6, ^6Li, is also a light element and known to have a high σ (940 barn). Li and B containing Ce-doped compounds, such as LiB_3O_5:Ce, $Li_2B_4O_7$:Ce [7], and a Cu-doped compound, $Li_2B_4O_7$:Cu [8,9] have been studied for use as neutron scintillation materials. $(Mg_{0.95}Mn_{0.05})_2B_2O_5$ was the first example of a neutron scintillator using Mn^{2+} as an activator.

The preparation of $LiMgBO_3$ and $LiMnBO_3$ has been reported by Lehmann et al. [10,11]. The crystal structures of monoclinic and hexagonal phases of $LiMnBO_3$ have been analyzed by Bondareva et al. [12] and Legagneur et al. [13], respectively. Norrestam has shown that the crystal structure of $LiMgBO_3$ is isotypic with monoclinic $LiMnBO_3$ (space group $C2/c$ (No. 15)) [14]. A number of reports on $LiMnBO_3$ as a cathode material for lithium batteries have recently been published [13,15]. There has been no report on the synthesis and luminescence of $LiMg_{1-x}Mn_xBO_3$ solid solutions. In the present paper, we synthesized the solid solutions, analyzed the crystal structures by X-ray diffraction (XRD), and characterized the photoluminescence (PL) properties.

2. Experimental

2.1. Synthesis of samples

The starting powders were Li_2CO_3 (99%, Wako Pure Chem. Ind.), MgO (99.9%, Rare Metallic), MnO (99.9%, Kojundo Chem. Lab.) and H_3BO_3 (99.99%,

* Corresponding author. Tel.: +81 22 217 5813; fax: +81 22 217 5813.
E-mail address: yamane@tagen.tohoku.ac.jp (H. Yamane).

0925-8388/$ – see front matter © 2011 Elsevier B.V. All rights reserved.
doi:10.1016/j.jallcom.2011.09.069

Sigma-Aldrich). MgO was heated at 900–1000 °C for 6–12 h before weighing. The powders were weighted with the molar ratios of Li_2CO_3:MgO:MnO:H_3BO_3 = 1:1–x:x:1:1 (x = 0–1.0) and mixed in an agate mortar with a pestle, and pressed into pellets in air. The pellets were placed on a platinum plate, and calcined at 750 °C for 6 h in an electric furnace under an Ar gas atmosphere. The obtained samples were powdered and pressed into pellets again, and heated at 800 °C for 12 h in Ar. Powder α-Fe (99.9%, Wako Pure Chem. Ind.) was used as an oxygen getter to prevent oxidation of Mn^{2+}.

Single crystals of $LiMg_{0.5}Mn_{0.5}BO_3$ were obtained from a polycrystalline sample of x = 0.5 using $LiBO_2$ as a flux. $LiBO_2$ was prepared in advance by heating Li_2CO_3 and H_3BO_3 at 750 °C for 6 h in air. The polycrystalline sample and a $LiBO_2$ flux were charged in a Pt boat and heated at 900 °C, and then cooled to 750 °C in Ar at a rate of −5 °C h^{-1}.

2.2. Characterization

The obtained polycrystalline pellets were powdered and XRD patterns of the powders were measured with a step width 0.02° using Cu $K\alpha$ radiation with a graphite monochromator mounted on a powder diffractometer (Rigaku, RINT2000). The unit cell parameters of the solid solutions were refined using the RIETAN-FP program [16].

XRD data of a single crystal were collected using Mo $K\alpha$ radiation with a graphite monochromator and an imaging plate on a single-crystal X-ray diffractometer (Rigaku, R-AXIS RAPID-II). Diffraction-data collection and unit-cell refinement were performed by the PROCESS-AUTO program [17]. Absorption correction was performed by the NUMABS program [18]. The crystal structure was refined by the full-matrix least-squares on F^2, using the SHELXL-97 program [19]. All calculations were carried out on a personal computer, using the WinGX software package [20]. The atomic coordinates were standardized by the STRUCTURE TIDY program [21]. The crystal structures were illustrated by the VESTA program [22]. The density of state of $LiMg_{0.5}Mn_{0.5}BO_3$ was calculated by the DV-Xα method using the SCAT code [23].

The PL excitation and emission spectra of the solid solutions were measured at room temperature with fluorescence spectrometers (Otsuka Electronics, Model QE-1000, JASCO, FP-6500) equipped with xenon lamps as excitation sources. A deuterium lamp and a fluorescence spectrometer (Bunkoukeiki Co., Ltd.) were used for the measurement of an excitation spectrum in the wavelength range λ_{ex} = 130–350 nm.

3. Results and discussion

3.1. $LiMg_{1-x}Mn_xBO_3$ solid solutions

Polycrystalline samples prepared by solid state reaction at 800 °C for 12 h were powdered for the powder XRD measurement. The reflections in the XRD patterns of the samples with x = 0.0–0.5 were indexed with monoclinic cell parameters of space group $C2/c$ (No. 15) Z = 8, as shown in Fig. 1a. Fig. 2 shows the results of cell parameter refinement by the Rietveld method using the structure model of $LiMgBO_3$ reported by Norrestam [14]. The cell volumes calculated from the parameters are plotted in Fig. 3. The cell parameters and volume of the sample of x = 0.0 were a = 5.1577(4) Å, b = 8.8847(11) Å, c = 9.9155(8) Å, β = 91.231(8)°, and V = 454.26(5) Å^3, which agreed with the previously reported parameters of $LiMgBO_3$ (a = 5.161(1) Å, b = 8.880(2) Å, c = 9.911(2) Å, β = 91.29(2)°, and V = 454.1(2) Å^3) [14]. The cell parameters, a, b, c, and β monotonously increased with increasing x as shown in Fig. 2.

The XRD patterns of the samples of 0.75 and 1.0 could be indexed with hexagonal cell parameters (Fig. 1c). The parameters refined with the model of $LiMnBO_3$ (space group $P\bar{6}$ (No. 174), Z = 3) were a = 8.1442(6) Å, c = 3.12481(15) Å, and V = 179.49(2) Å^3 for x = 0.75, and a = 8.1754(8) Å, c = 3.1489(2) Å, and V = 182.27(3) Å^3 for x = 1.0. The cell parameters of $LiMnBO_3$ were almost identical with those reported by Legagneur et al. (a = 8.172(1) Å, c = 3.1473(6) Å, and V = 182.02(8) Å^3) [13]. The 8/3 unit-cell volumes of the hexagonal samples were plotted on the extrapolated line of the monoclinic cells (Fig. 3), while the volume of the monoclinic $LiMnBO_3$ reported by Bondareva et al. [12] was smaller than the hexagonal phase.

3.2. Single crystal of $LiMg_{0.5}Mn_{0.5}BO_3$

Because of the severe preferred orientation of the (0 0 1) plane in the powder XRD patterns of the monoclinic phases (Fig. 1a and b), it was difficult to determine the atomic positions and displacement parameters precisely by the Rietveld method of the powder XRD pattern. Thus, single crystal XRD was carried out for the crystal prepared by slow cooling of the polycrystalline sample of x = 0.5 and a $LiBO_2$ flux from 900 °C. Colorless transparent platelet single crystals with the maximum size of 2 mm were obtained. The single crystal XRD data were collected for a platelet crystal of 0.4 mm × 0.3 mm × 0.1 mm.

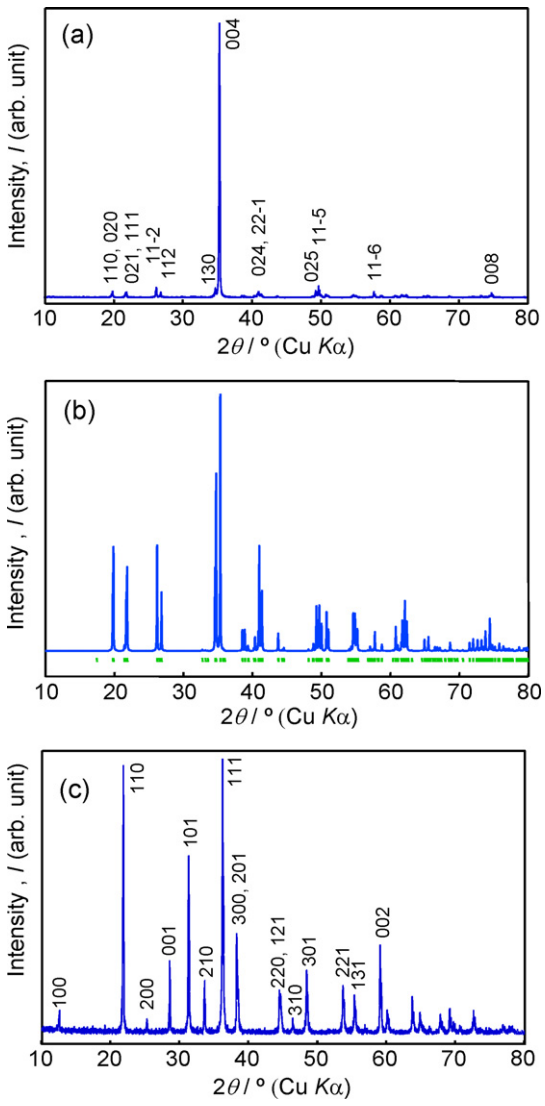

Fig. 1. XRD patterns of $LiMg_{1-x}Mn_xBO_3$, x = 0.50 observed (a) and calculated with a model refined by the single crystal XRD analysis of $LiMg_{0.5}Mn_{0.5}BO_3$ (b), and x = 0.75 observed (c).

The crystal data and structure refinement are shown in Table 1. Since the refined lattice parameters for the single crystal almost agreed with those measured for the polycrystalline sample of x = 0.5 as shown in Fig. 2, the composition of the single crystal was regarded as being $LiMg_{0.5}Mn_{0.5}BO_3$. The initial structure model used was based on the crystal structure of $LiMgBO_3$ reported by Norrestam [14]. In this model, the Li site was separated into two positions, and the atomic coordinates of x and y and isotropic displacement parameters U_{eq} were kept identical. The occupancies of the Li1 and Li2 sites of $LiMgBO_3$ were refined to be 0.57(5) and 0.43(5), respectively.

For the structure refinement of $LiMg_{0.5}Mn_{0.5}BO_3$, we fixed the occupancies of Li1 and Li2 sites as 0.5, and refined all positional parameters and anisotropic displacement parameters. Mg and Mn

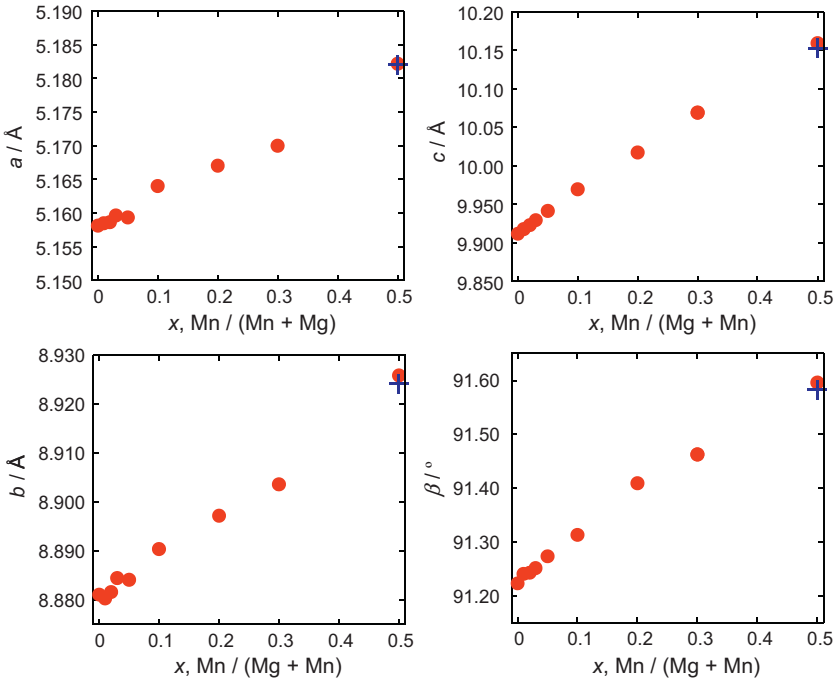

Fig. 2. Cell parameters of $LiMg_{1-x}Mn_xBO_3$ (x = 0.0–0.5) refined by powder X-ray diffraction (●) and those of $LiMg_{0.5}Mn_{0.5}BO_3$ by single crystal X-ray diffraction (+). The deviations are inside the marks.

atoms were statistically placed in an 8*f* site with the occupancy of 0.5. The anisotropic displacement ellipsoid of O3 was elongated almost along the *c*-axis direction and faced the split sites of Li1 and Li2. Thus, the original O3 site of $LiMgBO_3$ was also split into O3 and O4 sites with the occupancy of 0.5 for the structure of $LiMg_{0.5}Mn_{0.5}BO_3$. The final residual indices for all data were $R1 = 0.0271$, $wR2 = 0.0645$, and $S = 1.219$. The positions and anisotropic displacement parameters of Li, Mg/Mn, B and O atoms are listed in Tables 2 and 3. Figs. 4 and 5 show the coordination environments for the Li, Mg/Mn, and B atoms, and the crystal structure of $LiMg_{0.5}Mn_{0.5}BO_3$, respectively. While the Mn site is also divided into two positions in the structure of $LiMnBO_3$ reported by Bondareva et al. [12], the anisotropic displacement ellipsoid of the Mg1/Mn1 site in the structure of $LiMg_{0.5}Mn_{0.5}BO_3$ is close to a sphere shape (Fig. 4), indicating no need to separate the site.

Table 4 shows selected interatomic distances and O–B–O bond angles. All oxygen atoms in $LiMg_{0.5}Mn_{0.5}BO_3$ are bonded to B1 atoms and form planar triangular borate groups of BO_3. B–O bond lengths are 1.370(8)–1.3895(14) Å which are consistent with those reported for the structures of $LiMgBO_3$ [14], and $LiMnBO_3$ [12]. The bond valence sum (BVS) value for B [24,25] was calculated to be 2.899, which is close to the formal valence of B(III). The O–B–O bond angles are almost equal to 120°. The split sites of Li1 and

Table 1
Crystal data and structure refinement for $LiMg_{0.5}Mn_{0.5}BO_3$ with single crystal XRD data.

Chemical formula	$LiMg_{0.5}Mn_{0.5}BO_3$
Formula weight, M_r	210.75 g mol^{-1}
Temperature, T	298(2) K
Crystal system, space group	Monoclinic, $C2/c$ (No. 15)
Unit cell parameter	a = 5.1820(2) Å b = 8.9241(4) Å c = 10.1529(6) Å β = 91.5824(18)°
Unit-cell volume	469.34(4) Å^3
Z	8
Calculated density, D_{cal}	2.983 Mg m^{-3}
Radiation wavelength, λ	0.71075 Å (Mo $K\alpha$)
Absorption coefficient, μ	2.896 mm^{-1}
F_{000}	404
Crystal size	0.394 × 0.307 × 0.128 mm^3
θ range for data collection	4.02–30.52°
Limiting indices	$-6 \le h \le 7$, $-12 \le k \le 14$, $-14 \le l \le 14$
Reflections collected/unique	2779/720 [R(int) = 0.0379]
Absorption correction	Numerical
Data/restraints/parameters	720/0/73
Goodness-of-fit on F^2, S	1.219
R indices [$I > 2\sigma(I)$] $R1$, $wR2$	0.0258, 0.0636
R indices (all data) $R1$, $wR2$	0.0271, 0.0645
Largest diffr. peak and hole, $\Delta\rho$	0.484 and −0.414 e/Å^3

$R1 = \sigma||F_o| - |F_c||/\sigma|F_o|$. $wR2 = [\sigma w(F_o^2 - F_c^2)^2/\sigma(wF_o^2)^2]^{1/2}$, $w = 1/[\sigma^2(F_o^2) + (0.0366P)^2 + 0.1018P]$ where F_o is the observed structure factor, F_c is the calculated structure factor, σ is the standard deviation of F_o^2, and $P = (F_o^2 + 2F_c^2)/3$. $S = [\sigma w(F_o^2 - F_c^2)^2/(n-p)]^{1/2}$, where n is the number of reflections and p is the total number of parameters refined.

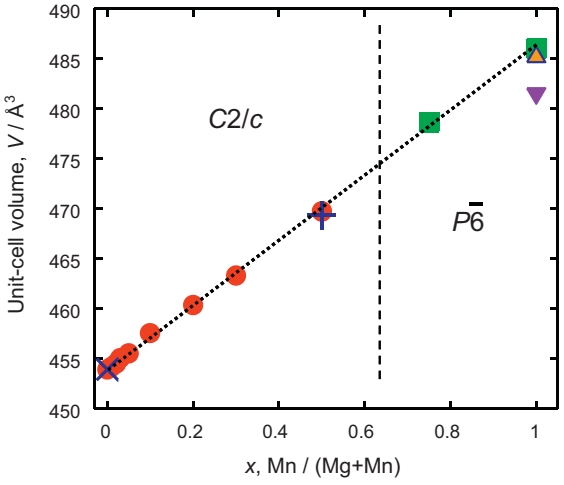

Fig. 3. Cell volumes of $LiMg_{1-x}Mn_xBO_3$ for Z = 8 versus Mn content, x, the monoclinic phases of the poly-crystals (●), and single crystal (+), hexagonal phases (■), and references $LiMgBO_3$ (×) [14], hexagonal $LiMnBO_3$ (▲) [13], and monoclinic $LiMnBO_3$ (▼) [12].

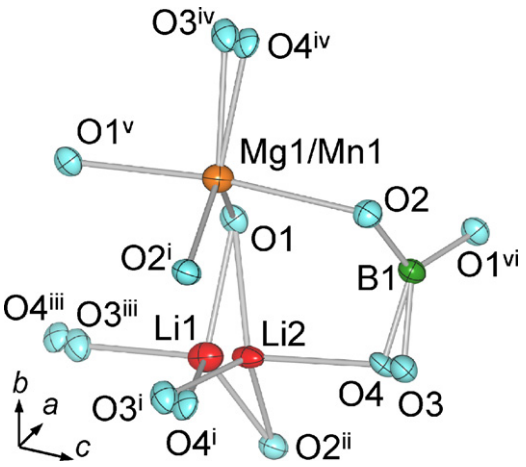

Fig. 4. Oxygen atom arrangement around Li, Mg1/Mn1 and B1 in the structure of $LiMg_{0.5}Mn_{0.5}BO_3$. Displacement ellipsoids are drawn at the 75% probability level. [Symmetry codes: (i) $-x, y, -z+1/2$; (ii) $-x+1/2, y-1/2, -z+1/2$; (iii) $x, -y, z-1/2$; (iv) $-x+1/2, y+1/2, -z+1/2$; (v) $-x+1/2, -y+1/2, -z$; (vi) $1-x, y, -z+1/2$.]

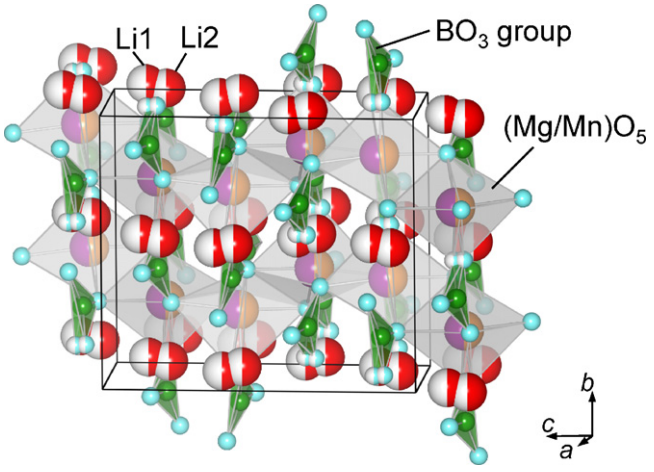

Fig. 5. Crystal structure of $LiMg_{0.5}Mn_{0.5}BO_3$ in a representation using cation-centered oxygen polyhedra.

Table 4
Selected bond lengths (Å) and angles (°) for $LiMg_{0.5}Mn_{0.5}BO_3$.

Li1–O2^{ii}	1.923(4)
Li1–O4^{i}	1.932(9)
Li1–O1	1.981(5)
Li1–O3^{iii}	2.096(7)
Avg. Li1–O	1.983
BVS[a]	1.005
Li2–O3^{i}	1.884(10)
Li2–O2^{ii}	1.919(4)
Li2–O1	2.002(4)
Li2–O4	2.053(7)
Avg. Li2–O	1.9645
BVS[a]	1.056
Mg1/Mn1–O4^{iv}	1.992(8)
Mg1/Mn1–O3^{iv}	2.033(8)
Mg1/Mn1–O1	2.0372(8)
Mg1/Mn1–O2^{i}	2.0583(8)
Mg1/Mn1–O1^{v}	2.1734(9)
Mg1/Mn1–O2	2.1930(8)
Avg. Mg1/Mn1–O	2.095
BVS[a] (Mg)	1.721
BVS[a] (Mn)	2.207
B1–O3	1.370(8)
B1–O4	1.375(8)
B1–O2	1.3892(14)
B1–O1^{vi}	1.3895(14)
Avg. B1–O	1.384
BVS[a]	2.899
O3–B1–O1^{vi}	118.5(4)
O4–B1–O1^{vi}	120.9(4)
O3–B1–O2	121.2(4)
O4–B1–O2	118.7(4)
O1^{vi}–B1–O2	119.87(9)

Symmetry codes: (i) $-x, y, -z+1/2$; (ii) $-x+1/2, y-1/2, -z+1/2$; (iii) $x, -y, z-1/2$; (iv) $-x+1/2, y+1/2, -z+1/2$; (v) $-x+1/2, -y+1/2, -z$; (vi) $1-x, y, -z+1/2$.

[a] BVS is defined as follows: $V_j = \sigma_i \exp[(l_0 - l_{ij})/B]$, where l_0 the bond valence parameters (BVP) presented by Brese and O'Keeffe [25] for B–O, Mg–O and Mn–O, l_{ij} is the distance between i and j atoms, and B is a constant value of 0.37 Å. The BVP values of the Li^+, Mg^{2+}, Mn^{2+}, and B^{3+} ions are 1.466, 1.693, 1.790, and 1.371 Å, respectively.

Table 2
Atomic coordinates and equivalent isotropic displacement parameter U_{eq} (Å^2) for $LiMg_{0.5}Mn_{0.5}BO_3$.

Atom Site	Occupancy	x	y	z	U_{eq}[a]	
Li1	8*f*	0.5	0.1592(9)	−0.0042(5)	0.0932(6)	0.0129(9)
Li2	8*f*	0.5	0.1649(9)	0.0111(5)	0.1574(5)	0.0098(8)
Mg1/Mn1	8*f*	0.5/0.5	0.16278(4)	0.33625(3)	0.12478(2)	0.00978(12)
B1	8*f*	1.0	0.3325(2)	0.17035(13)	0.37479(10)	0.0081(3)
O1	8*f*	1.0	0.40808(16)	0.16404(8)	0.08721(8)	0.00961(19)
O2	8*f*	1.0	0.22220(15)	0.30642(9)	0.33787(8)	0.00986(18)
O3	8*f*	0.5	0.1839(17)	0.0450(9)	0.3907(4)	0.0115(8)
O4	8*f*	0.5	0.1897(16)	0.0416(9)	0.3578(4)	0.0093(7)

[a] $U_{eq} = (\sigma_i \sigma_j U_{ij} a_i^* a_j^* \boldsymbol{a}_i \cdot \boldsymbol{a}_j)/3$.

Table 3
Anisotropic displacement parameters U_{ij} (Å^2) for $LiMg_{0.5}Mn_{0.5}BO_3$.

Atom	U_{11}	U_{22}	U_{33}	U_{12}	U_{13}	U_{23}
Li1	0.010(2)	0.011(2)	0.017(2)	0.0020(17)	0.0003(18)	0.0003(13)
Li2	0.0072(18)	0.0060(17)	0.016(2)	0.0023(16)	−0.0018(18)	−0.0004(12)
Mg1/Mn1	0.00917(18)	0.00931(17)	0.01093(17)	−0.00067(6)	0.00168(11)	0.00036(7)
B1	0.0069(6)	0.0080(6)	0.0094(5)	−0.0007(3)	0.0005(2)	−0.0001(3)
O1	0.0063(4)	0.0113(4)	0.0112(4)	−0.0005(2)	−0.0005(3)	0.0004(2)
O2	0.0096(4)	0.0085(3)	0.0114(4)	0.0003(3)	−0.0004(4)	0.0010(3)
O3	0.0121(11)	0.00101(10)	0.012(2)	0.0006(17)	−0.003(19)	−0.0022(8)
O4	0.0095(10)	0.0083(9)	0.010(2)	−0.0019(16)	−0.0018(18)	−0.0030(7)

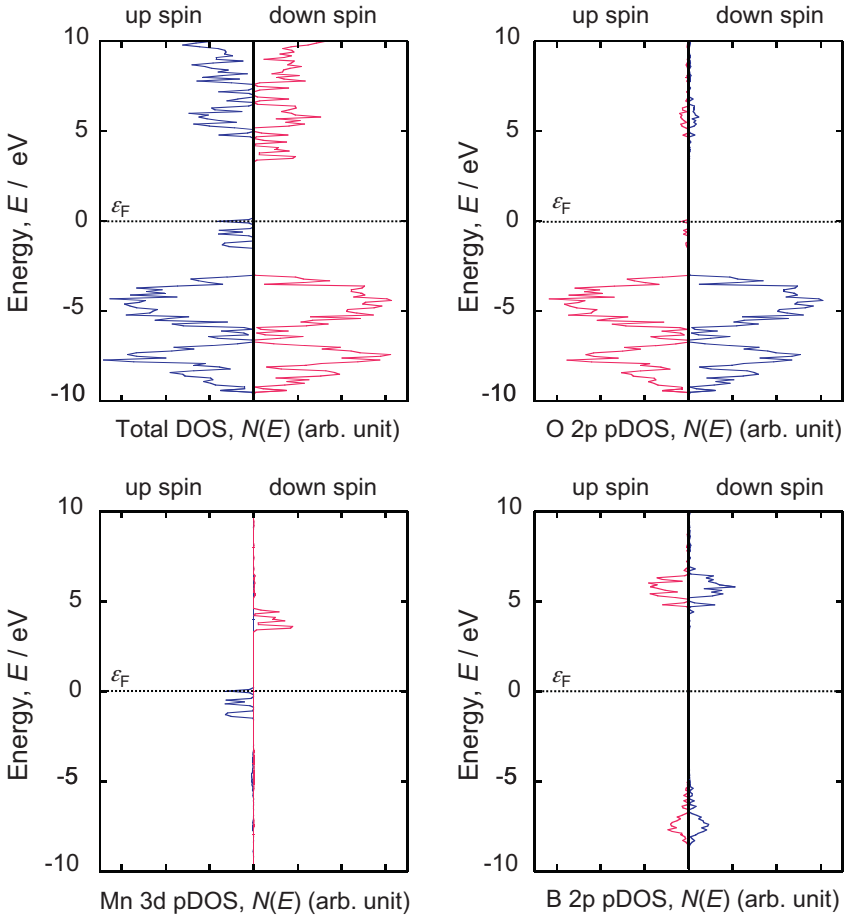

Fig. 6. Total density of states (DOS) and partial DOS for $LiMg_{0.5}Mn_{0.5}BO_3$. All curves have been shifted in energy so that Fermi energy ε_F indicated with a horizontal dotted line, lies at 0.0 eV.

Li2 are in the oxygen tetrahedra with Li1–O and Li2–O distances of 1.923(4)–2.096(7) Å and 1.884(10)–2.053(7) Å, respectively. The BVS values of Li1 and Li2 are 1.005 and 1.057, which correspond to the mono-valence of Li(I). The Mg1/Mn1 site is coordinated by five oxygen atoms of five BO_3 groups with Mg1/Mn1–O distances of 1.992(8)–2.1930(8) Å (average 2.095 Å). The BVSs of Mg and Mn were 1.721 and 2.207, respectively, suggesting that Mg–O and Mn–O bond lengths in the local structure are longer and shorter, respectively, than the length listed in Table 4. The average of the BVSs of Mg and Mn (1.964) is close to the formal valence of II for the Mg1/Mn1 site.

As shown in Fig. 5, Mg1/Mn1-site centered oxygen trigonal bipyramids share edges and form one-dimensional zigzag chains in the $[10\bar{1}]$ direction. These polyhedral chains are connected by B atoms, and Li atoms are inserted at the interstitials.

The electronic structure of the $[Li_{16}Mg_2Mn(BO_3)_{11}]^{11-}$ cluster which was placed in a Madelung potential was calculated by the DV-Xα method using the structure data of $LiMg_{0.5}Mn_{0.5}BO_3$. The average positions of Li1 and Li2, and O3 and O4 were used in the cluster model. The density of state (DOS) and partial DOS of $LiMg_{0.5}Mn_{0.5}BO_3$ estimated from the calculation are shown in Fig. 6. The highest-occupied molecular orbital (HOMO) mainly consists of an up-spin 3d orbital of Mn. A B2p–O2p band is above five unoccupied down-spin 3d orbitals of Mn.

3.3. Photoluminescence

The PL emission spectra of $LiMg_{1-x}Mn_xBO_3$ are shown in Fig. 7. Broad peaks of red emission were observed under excitation of 428 nm. The peak position in the spectra was at 696 nm for $x = 0.01$–0.10 and shifted to shorter wavelengths (blue shift) with increasing x: 693 nm ($x = 0.20$), 689 nm ($x = 0.30$), and 682 nm ($x = 0.50$). The relative emission intensities at 696 nm are shown in Fig. 8 as a function of x. The Mn content of the sample which shows the maximum intensity was around 0.10–0.20. A quantum efficiency of 4.8% was measured for the sample of $x = 0.20$. No emission was observed for the samples of

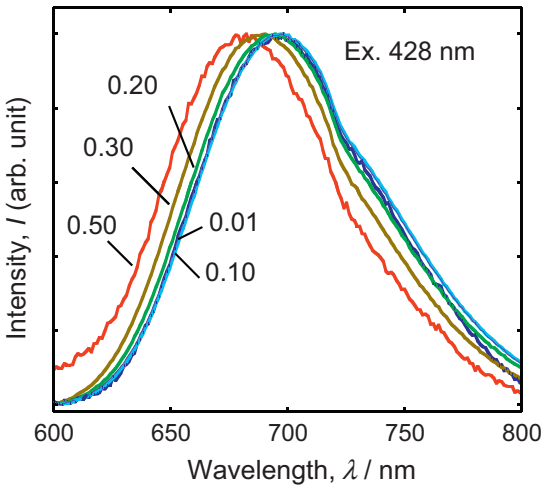

Fig. 7. PL emission spectra of $LiMg_{1-x}Mn_xBO_3$, $x = 0.01$–0.50.

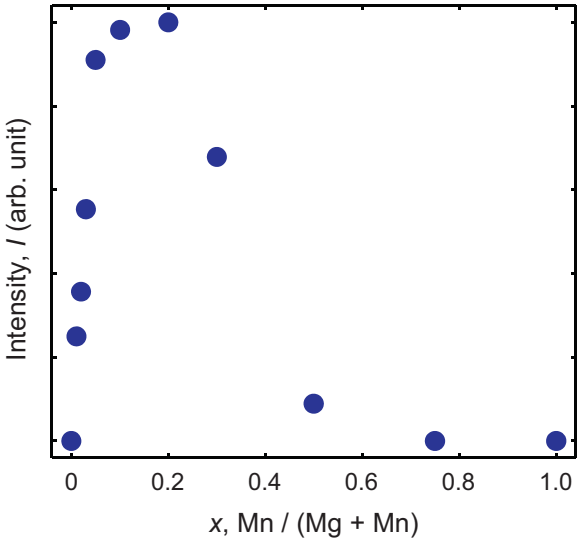

Fig. 8. Relative emission intensities of $LiMg_{1-x}Mn_xBO_3$ versus the Mn content x.

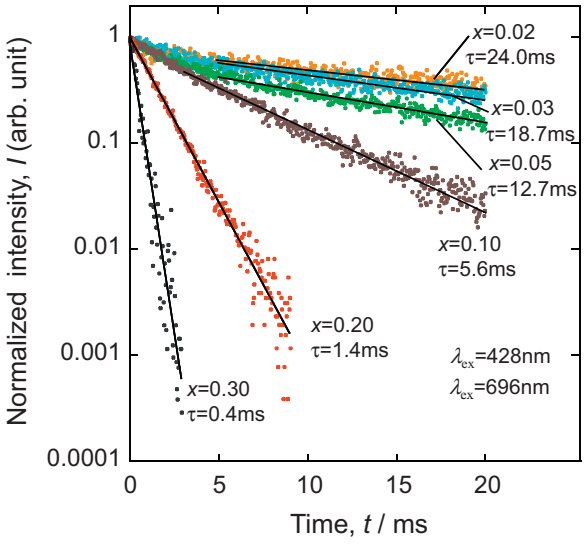

Fig. 9. Normalized photoluminescence decay curve of $LiMg_{1-x}Mn_xBO_3$, $x = 0.02–0.30$ (excited at 428 nm, monitored at 696 nm).

the hexagonal phases ($x = 0.75$ and 1.0). Similar red emission by Mn^{2+} doping was reported for $(Mg_{1-x}Mn_x)_2B_2O_5$ (670 nm, $x = 0.05–0.20$) [5], $MgSiO_3$:Mn^{2+} (660–685 nm, Mn^{2+} 1–3%) [26–28], and Mg_2SiO_4:Mn^{2+} (650–660 nm, Mn^{2+} 1–3%, 647 and 748 nm, Mn^{2+} 4%) [27,29]. In these compounds, Mn^{2+} was doped in a 6-fold oxygen octahedral site.

The coordination numbers for Mn^{2+} in the phosphor materials listed by Tamatani [2] are 4, 6, and 8. In his review, 5-fold coordinated Mn^{2+} ions in $SrAl_{12}O_{19}$ and $CaAl_{12}O_{18}$ studied by Bergstein and White [30] were introduced. There are 4-, 5-, 6-, and 12-fold sites in these compounds. The emission peaks at 515, 560, and 590 nm from the 0.02 mol% Mn^{2+}-doped $SrAl_{12}O_{19}$ were associated with Mn^{2+} in the 4-fold, 5-fold, and 12-fold Al^{3+} sites, respectively. However, the doping of Mn^{2+} into the oxygen trigonal bipyramid 5-fold Al^{3+} site was assumed and not confirmed experimentally. Another example of the emission from 5-coordinated Mn^{2+} not in solid state inorganic materials, but in a polymer $[Mn(Hbidc)]_n$ (Hbidc = 1*H*-benzimidazole-5,6-dicarboxylate) was found [31]. Mn^{2+} is coordinated by four oxygen and one nitrogen in the polymer, which emits red luminescence ($\lambda_{em} = 726$ nm) under excition of d–d transition at around 420 nm and a metal-to-ligand charge-transfer excited state at 250–350 nm [31].

Fig. 9 shows PL decay curves of Mn^{2+} in $LiMg_{1-x}Mn_xBO_3$. Relatively rapid decays were observed up to about 5 ms for the samples of $x = 0.02–0.1$. In this composition range, the emission intensity increased with x (Fig. 8). The decay times (τ) calculated by exponential fitting after 5 ms decreased from 24.0 to 5.6 ms with increasing x. Simple exponential decay was observed for the samples of $x = 0.20$ and 0.30 where concentration quenching occurred. The decay times of the samples of $x = 0.20$ and 0.30 were 1.4 and 0.4 ms, respectively.

The dependence of the decay time on the Mn^{2+} concentration of Zn_2SiO_4:Mn was analyzed in terms of optical transitions on isolated Mn^{2+} ion and on Mn^{2+} ion pairs [32]. Mn^{2+} was doped in the 4-fold tetrahedral Zn^{2+} site of Zn_2SiO_4. A red shift of the green emission peak from 519 to 526 nm was observed with increasing Mn^{2+} concentration x of $Zn_{2(1-x)}Mn_{2x}SiO_4$ from 0.0005 to 0.125. Ronda and Amrein explained the shortening of the decay time and the red shift of Zn_2SiO_4:Mn with increasing x, assuming an exchange interaction between Mn^{2+} ions [33]. Red shifts with increasing Mn^{2+} content were also reported for the red emission of $MgSiO_3$:Mn^{2+} (660–685 nm, Mn^{2+} 1–3%) [27] and Mg_2SiO_4:Mn^{2+} (650–660 nm, Mn^{2+} 1–3%) [27,29]. It was unclear whether the decay time dependence and the blue shift of the red emission observed for $LiMg_{1-x}Mn_xBO_3$ were also explained by the exchange interaction.

The PL excitation spectrum of $LiMg_{0.90}Mn_{0.10}BO_3$ is shown in Fig. 10. The small broad peaks observed from around 250–600 nm can be ascribed to d–d transition of Mn^{2+}. The d–d absorption peaks of Mn^{2+} at octahedral or tetrahedral sites are usually sharp and assigned using the Tanabe–Sugano diagram. However, owing to the broadness of the peaks, they could not clearly be labeled using the diagram. The broad peaks observed at around 580 nm, 428 nm, 374 nm, and 248 nm for $LiMg_{0.90}Mn_{0.10}BO_3$ might correspond to $^4T_{1g}(G)$ (572 nm), $^4T_{2g}(G)$ (433 nm) and $^4A_{1g}/^4E_g(G)$ (416 nm), $^4T_{2g}(D)$ (372 nm) and $^4E_g(D)$ (351 nm), and $^4A_{2g}(F)$ (242 nm) observed for $(Mg_{0.95}Mn_{0.05})_2B_2O_5$ [5]. The strong excitation peak below 240 nm could be attributed to the spin allowed transition from up-spin Mn 3d to the unoccupied B2p–O2p band. The emission intensity excited at 200 nm was over six times higher than that excited at 428 nm.

$LiMg_{1-x}Mn_xBO_3$ solid solutions prepared with ^{10}B and ^6Li are expected to be a neutron scintillator material with low γ-ray noise similar to $(Mg_{0.95}Mn_{0.05})_2B_2O_5$. Their combination with Si photodiode could also be possible because of the red emission of 696 nm.

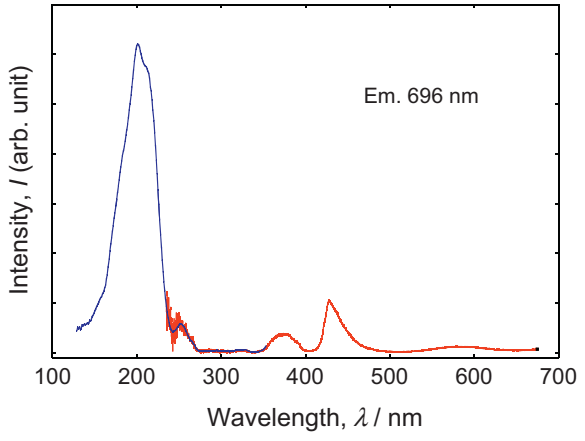

Fig. 10. PL excitation spectrum of $LiMg_{0.90}Mn_{0.10}BO_3$.

4. Conclusions

Monoclinic ($C2/c$) and hexagonal ($P\bar{6}$) phases of $LiMg_{1-x}Mn_xBO_3$ were prepared at 800 °C in Ar by solid state reaction at $0 \leq x \leq 0.5$ and $0.75 \leq x \leq 1.0$, respectively. Mn^{2+} in the monoclinic phase is coordinated by 5 oxygen atoms and situated in an oxygen trigonal bipyramid. Red light with a peak of 682–696 nm (decay time 0.4–24 ms) was emitted from the monoclinic solid solutions by excitation of Mn d–d transition (λ_{ex} = 428 nm) and by ultraviolet light irradiation (λ_{ex} = 200 nm). Concentration quenching was observed for the samples from x = 0.20.

Acknowledgments

This work was supported in part by a Grant-in-Aid for Scientific Research (B) (No. 21350113, 2009) and the Global COE Program "Materials Integration, Tohoku University" from the Ministry of Education, Culture, Sports and Technology (MEXT), Japan.

Appendix A. Supplementary data

Supplementary data associated with this article can be found, in the online version, at doi:10.1016/j.jallcom.2011.09.069.

References

[1] F.A. Kröger, Some Aspects of the Luminescence of Solids, Elsevier, Amsterdam, 1948, pp. 57–106.
[2] M. Tamatani, in: W.M. Yen, S. Shionoya, H. Yamamoto (Eds.), Phosphor Handbook, 2nd ed., CRC Press, Boca Raton, FL, 2007, pp. 183–187.
[3] T.H.P.J. Botden, F.A. Kröger, Physica 8 (1947) 216–224.
[4] R. Dittmann, D. Hahn, U. Müller, J. Lumin. 3 (1970) 230–239.
[5] T. Kawano, T. Suehiro, T. Sato, H. Yamane, J. Lumin. 130 (2010) 2161–2165.
[6] K. Fukuda, T. Kawano, H. Yamane, T. Yanagida, N. Kawaguchi, Y. Fujimoto, A. Yoshikawa, Ext. Abstr. [58th Spring Meet. 2011], Jpn. Soc. Appl. Phys. Rel. Soc., 26p-EA-4, 2011 (in Japanese).
[7] C.W.E. Eijk, Nucl. Instrum. Methods Phys. Res. A 460 (2001) 1–14.
[8] M. Ishii, Y. Kuwano, H. Sato, S. Tanaka, M. Kobayashi, T. Oku, T. Adachi, K. Sakai, H.M. Shimizu, J. Suzuki, N. Senguttuvan, K. Susa, J. Jpn. Assoc. Cryst. Growth 29 (2002) 7.
[9] M. Ishii, Y. Kuwano, T. Asai, N. Senguttuvan, T. Hayashi, M. Kobayashi, T. Oku, K. Sakai, H.M. Shimizu, J. Suzuki, J. Cryst. Growth 257 (2003) 169–176.
[10] H.-A. Lehmann, H. Schadow, H.-J. Papenfuss, Z. Anorg, Allg. Chem. 314 (1962) 159–166.
[11] H.-A. Lehmann, H. Schadow, Z. Anorg, Allg. Chem. 348 (1966) 42–49.
[12] O.S. Bondareva, M.A. Simnov, Y.K. Egorov-Tismenko, N.V. Belov, Sov. Phys. Crystallogr. 23 (1978) 269–273.
[13] V. Legagneur, Y. An, A. Mosbah, R. Portal, A.L.G.L. Salle, A. Verbaere, D. Guyomard, Y. Piffard, Solid State Ionics 139 (2001) 37–46.
[14] R. Norrestam, Z. Kristallogr. 187 (1989) 103–110.
[15] L. Chen, Y. Zhao, X. An, J. Liu, Y. Dong, Y. Chen, Q. Kuang, J. Alloys Compd. 494 (2010) 415–419;
V. Aravindan, K. Karthileyan, S. Amaresh, Y.S. Lee, Bull. Korean Chem. Soc. 31 (2010) 1506–1508;
G. Liu, Q. Wu, B. Ma, Adv. Mater. Res. 197–198 (2011) 526–530;
J.C. Kim, C.J. Moore, B. Kang, G. Hautier, A. Jain, G. Ceder, J. Electrochem. Soc. 158 (2011) A309–A315.
[16] F. Izumi, K. Momma, Solid State Phenom. 130 (2007) 15–20.
[17] PROCESS-AUTO; Rigaku/MSC & Rigaku Corporation: The Woodlands, TX, USA and Akishima, Tokyo, Japan, 2005.
[18] T. Higashi, NUMABS-Numerical Absorption Correction, Rigaku Corporation, Tokyo, 1999.
[19] G.M. Sheldrick, Acta Crystallogr., Sect. A: Found. Crystallogr. 64 (2008) 112–122.
[20] L.J. Farrugia, J. Appl. Crystallogr. 32 (1999) 837–838.
[21] L.M. Gelato, E. Parthé, J. Appl. Crystallogr. 20 (1987) 139–143.
[22] K. Momma, F. Izumi, J. Appl. Crystallogr. 41 (2008) 653–658.
[23] H. Adachi, M. Tsukada, C. Satoko, J. Phys. Soc. Jpn. 45 (1978) 875–883.
[24] I.D. Brown, D. Altermatt, Acta Crystallogr., Sect. B: Struct. Sci. 41 (1985) 244–247.
[25] N.E. Brese, M. O'Keeffe, Acta Crystallogr., Sect. B: Struct. Sci. 47 (1991) 192–197.
[26] X.-J. Wang, D. Jia, W.M. Yen, J. Lumin. 102–103 (2003) 34–37.
[27] L. Lin, M. Yin, C. Shi, W. Zhang, J. Rare Earths 24 (2006) 104–107.
[28] L. Lin, C. Shi, Z. Wang, W. Zhang, M. Yin, J. Alloys Compd. 466 (2008) 546–550.
[29] L. Lin, M. Yin, C. Shi, W. Zhang, J. Alloys Compd. 455 (2008) 327–330.
[30] A. Bergstein, W.B. White, J. Electrochem. Soc. 118 (1971) 1166–1171.
[31] Y. Wei, Y. Yu, K. Wu, Cryst. Growth Des. 8 (2008) 2087–2089.
[32] C. Barthou, J. Benoit, P. Benalloul, J. Electrochem. Soc. 141 (1994) 524–528.
[33] C.R. Ronda, T. Amrein, J. Lumin. 69 (1996) 245–248.